JOURNAL OF GEOPHYSICAL RESEARCH, VOL. 103, NO. B10, PAGES 24,321–24,331, OCTOBER 10, 1998

Quasi-Love phases between Tonga and Hawaii: Observations, simulations, and explanations

Vadim Levin and Jeffrey Park

Department of Geology and Geophysics
Yale University, New Haven, Connecticut

Abstract.

Seismograms of some shallow Tonga earthquakes observed at Hawaii contain SV-polarized phases in the Love wave time window, most prominently on the vertical component. Given the geometry of the observations ($\Delta \approx 40 - 45°$), such phases may be explained either as body waves or as mode-converted surface waves. Detailed synthetic seismogram modeling of representative events reveals several instances where the body wave explanation is inadequate, even when plausible uncertainties in the source mechanism are taken into account. The observed SV-polarized phase can instead be generated through Love-Rayleigh scattering, which requires laterally varying seismic anisotropy along the Tonga-Hawaii path. Trial-and-error forward modeling with simple structures based on the transversely isotropic mid-Pacific velocity model PA5 of *Gaherty et al.* [1996] obtains velocity structure that yields synthetic seismograms matching the observations. This model, while non unique, suggests first-order constraints on the lateral variation in anisotropic properties, and associated mantle flow, along the Tonga-Hawaii path. By examining trade-offs in model parameters, we conclude that robust features of the model are: (1) a transition from radial to mixed radial and azimuthal anisotropy 3°–5° from Hawaii; (2) the NW-SE alignment of the axis of azimuthal anisotropy; (3) higher degree of P anisotropy relative to S anisotropy; and (4) the presence of azimuthal anisotropy within upper 200-250 km of the mantle. Taken together, these features imply a disruption of mantle fabric by the processes forming Hawaii-Emperor volcanic system. A model with anisotropic gradients in both the lithospheric lid and shallow asthenosphere is the simplest extension of our starting model. However, an equivalent data fit can be obtained if the azimuthal-anisotropy gradients are restricted to line beneath the high-velocity "lid" of model PA5, so that mantle hot spot flow need not penetrate the lithospheric lid.

1. Introduction

Earthquakes in the Tonga-Fiji region observed by stations Honolulu (HON) and Kipapa (KIP) on the Hawaiian island of Oahu have fueled numerous studies of the Pacific lithosphere [*Jordan and Sipkin* 1977; *Revenaugh and Jordan*, 1987; *Gaherty et al.*, 1996; *Katzman et al.*, 1997]. Among the attractive features of this geometry (Figure 1) are numerous events that provide abundant data and their distribution in depth, which leads to a wealth of observed seismic phases. The relative simplicity of the propagation path invites the use of simple models.

The great circle path from the Tonga subduction zone to Hawaii samples oceanic lithosphere formed during the Cretaceous Long Normal polarity interval (sometimes referred to as the Superchron) between 80 and 100 Ma [*Helsley and Steiner*, 1969]. The bathymetry along the path is slightly in excess of 5 km on average, which is somewhat shallow given the age and a simple model of boundary layer cooling [e.g., *Anderson* 1989]. It should be noted that more complex models do accommodate the observed bathymetry in the Pacific (see, e.g., *Renkin and Sclater*, [1988] for a discussion).

The path crosses part of the Darwin Rise, a region of Cretaceous volcanism, crustal rejuvenation, and uplift [*Menard*, 1984]. A modern-day region of broad-scale volcanic activity, the Pacific Superswell [*McNutt and Fischer*, 1987], is located farther to the southeast. In spite of past volcanic activity, the present-day combination of bathymetry and heat flow along the path is not exceptional with respect to other oceanic regions [*Stein and Stein*, 1993], which suggests that the lithosphere was reheated after formation and has been subsiding since. Lacking magnetic lineation evidence, the features of the region's bathymetry are the best guide

Paper number 98JB02342.
0148-0227/98/98JB-02342$09.00

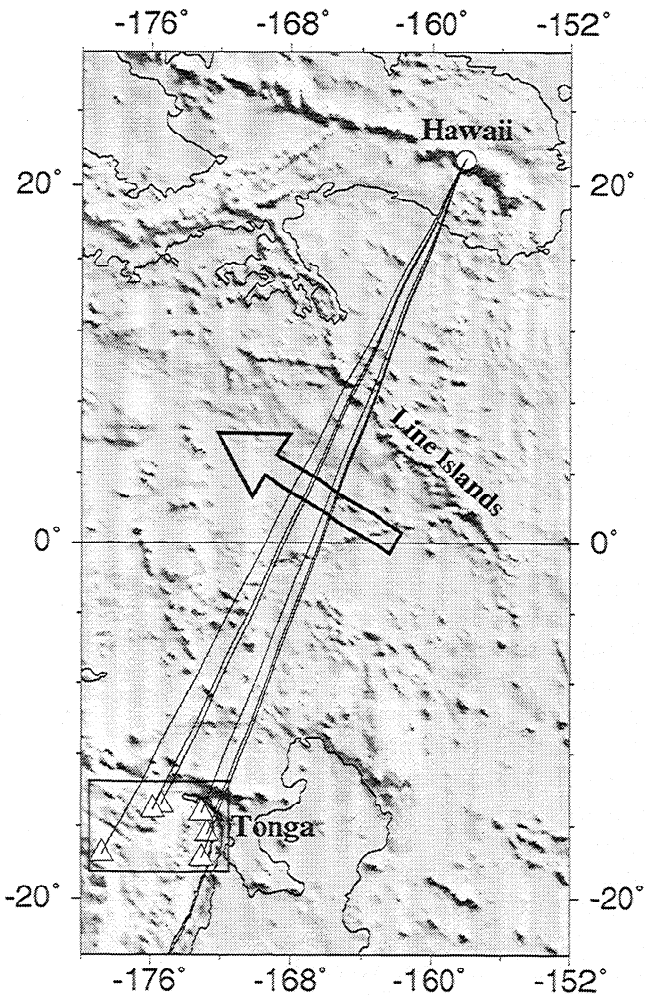

Figure 1. An overview map of the Tonga-Hawaii corridor in the western Pacific. The station KIP is denoted by a circle; earthquakes are shown by triangles. A bathymetric level of 5100 m is shown by a solid line. The large arrow indicates plate motion direction. The small box surrounding the source region corresponds to the frame of Figure 3. Digital bathymetry data are from ETOPO-5 data set.

to the tectonic history of the lithosphere. The present-day plate motion is nearly normal to the Tonga-Hawaii path, as prominently recorded by the Hawaiian hot spot track (Figure 1). Present-day plate motion also appears to be recorded in the alignment of olivine crystals in the lithosphere midway along the path, as inferred from the splitting of PS waves in records of deep Tonga-Fiji events [*Su and Park*, 1994]. The Line Islands, aligned more north-south, reflect an earlier plate motion direction.

Gaherty et al., [1996] proposed a detailed one-dimensional profile of seismic properties for the Tonga-Hawaii corridor, the PA5 model. Similar to the preliminary reference Earth model (PREM) [*Dziewonski and Anderson*, 1981], their velocity structure includes seismic anisotropy with a vertical axis of hexagonal symmetry in the lithospheric layer between the depths of 12 km and 166 km, encompassing both the high-velocity lithospheric "lid" and the underlying asthenosphere. As shown below, synthetic seismograms computed for the PA5 structure match well the main surface wave groups observed at Oahu (Global Seismic Network (GSN) station KIP), allowing us to explore more subtle features of the long-period data. Specifically, we examine phases arriving in the Love wave time window on the vertical and radial components. Given the geometry of the observations, such phases may be explained either as body waves or as scattered surface waves.

The candidate body waves are of the multiply reflected S families (SS, $SnSn$). The PA5 model of *Gaherty et al.* [1996] is partially based on observations of these phase families; therefore they should be well reproduced in synthetic seismograms. The candidate surface wave would be a Love-to-Rayleigh converted phase (termed "quasi-Love" by *Park and Yu* [1992] and denoted qL hereinafter) that arises through mode conversion of the long-period fundamental Love surface wave at strong lateral gradients in upper mantle anisotropy. Since fundamental Love and Rayleigh waves have distinct group velocities at a common frequency, the timing of a scattered Rayleigh wave, relative to Love, can be used to localize the anisotropic gradient. The qL waves are well suited for the study of the oceanic interiors, where stations are sparse and tomographic lateral resolution depends on long crossing paths. It is of significant interest to investigate if the phases that we observe in records of shallow earthquakes in the Tonga region are indeed qL phases, in which case they would provide new information on the anisotropic structure along the Tonga-Hawaii path.

Through detailed synthetic seismogram modeling we investigate the nature of observed waveforms of representative events and show that both of the above mechanisms can contribute to the phase in question. The relative contributions from body and mode-converted surface waves depend on the earthquake hypocenter and source mechanism. By matching synthetic seismograms to observations we develop a simple model of laterally varying anisotropy for the path between Tonga and Hawaii. The model suggests a significant disruption of spreading-related mantle fabric in the vicinity of Hawaii.

2. Observed Waveforms

For a number of earthquakes in the Tonga region recorded by station KIP, a long-period phase arrives on the vertical and radial components, generally synchronous with the Love ($G1$) wave. This phase is prominent if the observation is made near the Rayleigh wave radiation node of the source, where it is similar in amplitude to the Rayleigh ($R1$) wave. Figure 2 shows records, low-pass filtered at 50 s, of four such events from the Tonga region, all displaying a pronounced phase ahead of the $R1$. Notice the similarity in the observed wave-

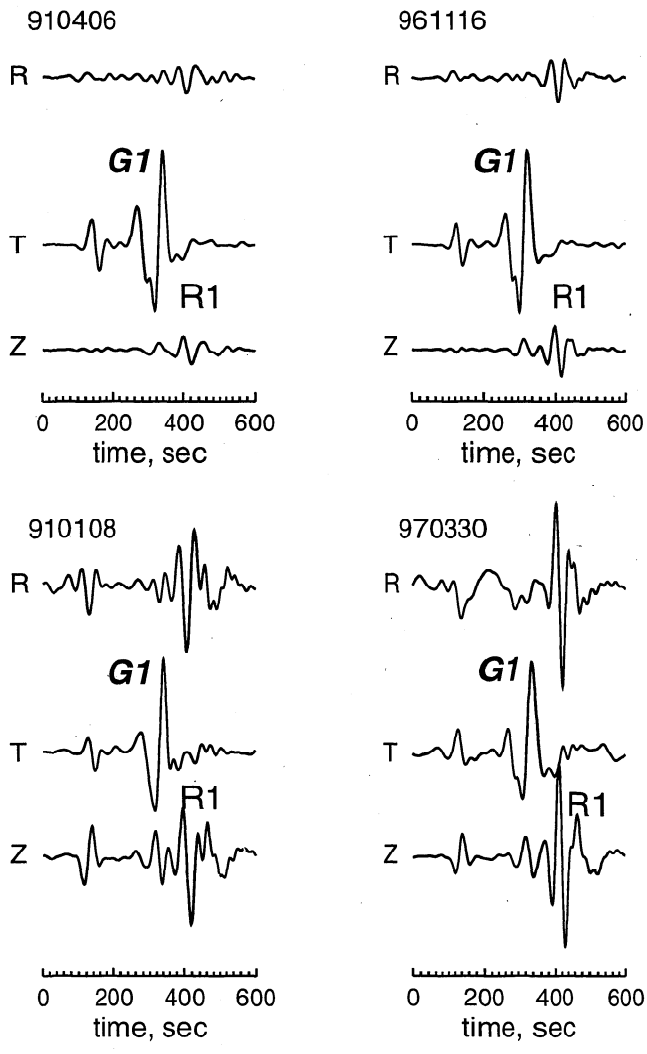

Figure 2. Waveforms of four earthquakes in Tonga region that display SV-polarized phases in the Love wave time window. Low-pass filter at 0.02 Hz is applied to all waveforms. Thin vertical lines show time windows used in particle motion plots of Figure 4. $G1$ and $R1$ denote Love and Rayleigh waves, respectively, traveling directly from the source to the receiver.

forms of major surface phases. Clearly, in all four cases the Love wave time window contains both SV- and SH-type motion. Such motion cannot be explained by sidewise refraction or multipathing of Love waves, as their motion would be restricted to the horizontal plane. Therefore an additional phase, nearly synchronous with $G1$ and similar in amplitude to $R1$, is present.

The locations and focal mechanisms of these earthquakes are shown on Figure 3. Their source parameters are taken from the Harvard centroid moment tensor (CMT) catalog (Table 1). Two events have strike-slip mechanisms, while the other two are of a predominantly thrust character. All four are oriented so that the nodal plane of the double-couple solution aligns approximately with the direction toward Hawaii, resulting in low-amplitude Rayleigh waves. For two events, one strike-slip and one thrust, Figure 4 illustrates the particle motion of the phase we are interested in. Within the Love wave arrival window (marked by vertical lines on Figure 2), event 910108 (a thrust) has wide elliptical particle motion in the radial-vertical (SV) plane, as well as in transverse-vertical (SH) plane. Overall, the amplitude of the SV-polarized phase is ~30% of the Love wave. Event 910406 (a strike-slip) has an SV-polarized phase ~10% of the Love wave in amplitude, with a more complex particle motion in the SV plane. Owing to the similarity in source-receiver distances and the overall path structure, major phases ($G1$ and $R1$) of these two events bear close resemblance, while the two SV-polarized phases in Love time window appear to be quite different, both in relative amplitude and in particle motion.

3. Synthetic Seismograms in an Anisotropic Earth

To compute synthetic seismograms, we apply the path-integral asymptotics of [*Park*, 1997, 1998] to include constant and laterally variable anisotropy in synthetic seismograms. We restrict attention to anisotropic models with hexagonal symmetry about a single axis $\hat{\mathbf{w}}$. Individual olivine crystals possess a more complex orthorhombic symmetry [*Anderson*, 1989]. Our assumption of a single symmetry axis implies systematic preferred orientation of only one olivine crystal axis (the "fast" a axis) during the deformation of mantle peridotite in the ocean lithosphere. A complex nomenclature has grown up around different types of anisotropy, associated with the orientation of $\hat{\mathbf{w}}$, or the presence of higher complexity in the 4th-order tensor that relates stress and strain in elastic media. In this report, we use terms "radial" or "radially symmetric" to denote anisotropic media in which $\hat{\mathbf{w}}$ is vertical, or else to denote the portion of the stress-strain tensor that can be represented with vertical $\hat{\mathbf{w}}$. We use the term "azimuthal" to denote anisotropic medium in which the symmetry axis $\hat{\mathbf{w}}$ is horizontal, or else to denote the portion of the stress-strain tensor that can be represented with horizontal $\hat{\mathbf{w}}$. In this paper we do not consider cases where the symmetry axis is inclined between horizontal and vertical; note that the stress-strain tensor in such cases does not separate into portions with $\hat{\mathbf{w}}$ vertical and $\hat{\mathbf{w}}$ horizontal. Nevertheless, we do consider models with combinations of radial and azimuthal anisotropies in order to simulate portions of the upper mantle that may possess more complex fabric, e.g., near the Hawaii hot spot. It is tempting, but not straightforward, to relate such composite models to the orthorhombic symmetry appropriate for single olivine crystals, for which the three coordinate axes have distinct seismic velocities.

For media with a symmetry axis $\hat{\mathbf{w}}$, seismic velocities of plane waves depend on the angle η between the wavenumber vector $\mathbf{k}$ and $\hat{\mathbf{w}}$. If both $\hat{\mathbf{w}}$ and $\mathbf{k}$ are

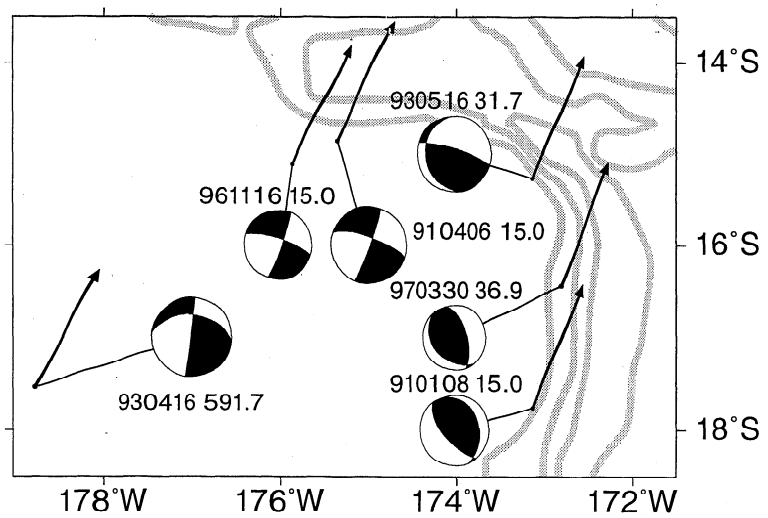

Figure 3. Hypocentral locations and mechanisms of earthquakes used in this work. Bathymetric levels of 6000, 4500, and 3000 m are shown by thick grey lines. Compressional quadrants of focal mechanisms are shaded. Arrows denote great circle directions toward Hawaii.

horizontal in a flat-layered medium, perturbations to the P and SV velocities vary according to the formulas [*Backus*, 1965; *Park*, 1993]

$$\begin{aligned} \delta(\alpha^2)/\alpha_0^2 &= A + B\cos 2\eta + C\cos 4\eta \\ \delta(\beta^2)/\beta_0^2 &= D + E\cos 2\eta. \end{aligned} \quad (1)$$

If density perturbations are neglected, knowledge of A, B, C, D, E is sufficient to determine the perturbation to the elastic tensor [*Shearer and Orcutt*, 1986]. An arbitrary orientation of $\hat{\mathbf{w}}$ can be applied by rotating the tensor. We will concentrate on the anisotropic parameters B and E, as both are demonstrably nonzero in the upper mantle.

We grafted an isotropic average of the PA5 model [*Gaherty et al.*, 1996] onto the lower mantle and core of PREM as the reference for free oscillations on a spherical earth. The depth-dependent anisotropic features of the model PA5 are represented using a Legendre polynomial approximation up to the order 5 but with a constant ratio $B/E = 0.5$. The use of the PA5 upper mantle velocity structure proved critical for successful representation of $G1$ and $R1$ phases in observed seismograms. Shear and compressional anisotropy vary independently in PA5, but this does not appear to exert a significant influence on the long-period surface waves used in this study. Vertical profiles of velocity and anisotropy variation with depth in PA5 and in our model are shown in Figure 5.

4. Body Waves in a 1D Structure

Given the geometry of observations (shallow sources at distances $\sim 40°$) candidate body phases for the observed phenomena would be SS, SSS, and $SnSn$. Figure 6 illustrates the time relationship between the Love wave and multiple S waves for a broad range of distances. Data records with similar behavior were reported by *Gaherty et al.* [1996], with multiple S waves being the preferred explanation.

If the waveform present in the Love wave window of Figure 2 is a body wave, it should also be present in synthetic seismograms computed for a radially symmetric Earth model. We test this expectation by com-

Table 1. Hypocentral Parameters of Earthquakes Used in This Work From the CMT Catalog

Date (Event)	Origin Time, UT	Latitude °S	Longitude °W	Depth km	Moment, $\times 10^{25}$	BAZ deg	Δ, deg
Jan. 8, 1991 (910108)	22 04:19.0	17.76	173.12	15 (43)	1.98	202.39	42.31
April 6, 1991 (910406)	14 34:28.2	14.86	175.36	15	11.11	206.79	40.32
April 16, 1993 (930416)*	14 08:46.7	17.54	178.76	591.7	26.2	209.12	43.95
May 16, 1993 (930516)*	21 44:58.9	15.27	173.12	31.7	8.91	203.52	39.72
Nov. 16, 1996 (961116)	09 47:54.2	15.11	175.86	15.0	0.93	207.68	40.69
March 30, 1997 (970330)	08 38:34.8	16.44	172.83	36.9	0.35	202.16	40.55

Depth in parentheses is from the NEIC catalog. Backazimuth (BAZ) and epicentral distance (Δ) values are for the station KIP.

*events used for model verification only.

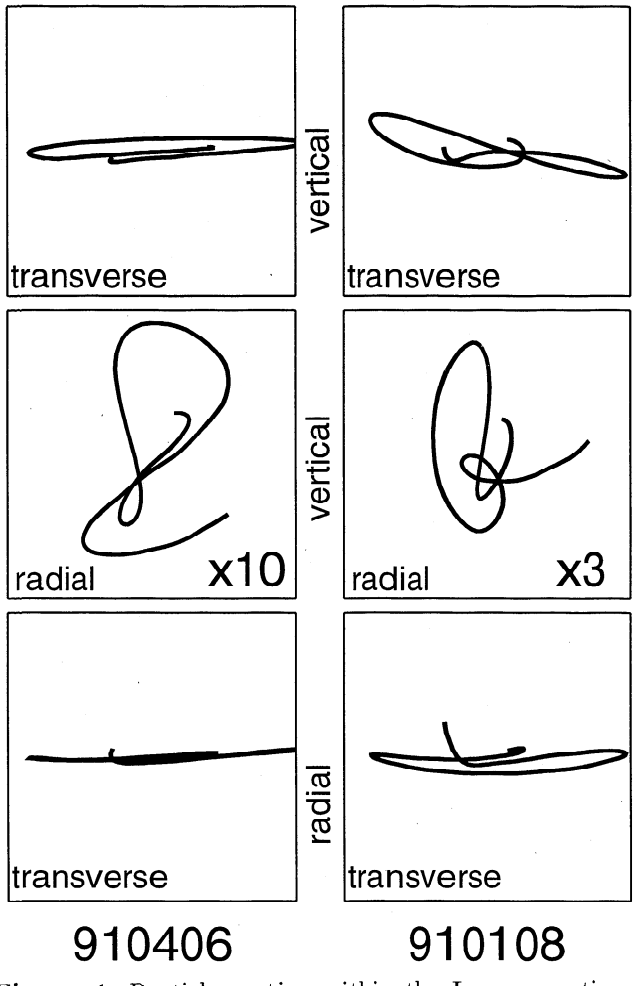

Figure 4. Particle motion within the Love wave time frame for two representative events. Time windows used are marked on Figure 2 by thin vertical lines. Radial-vertical plots are enlarged to show detail. A thrust mechanism (January 8, 1991, event 910108) produces transverse motion 3 times larger then the vertical, while the strike-slip (April 6, 1991, event 910406) yields transverse motion almost 10 times the vertical. Particle motion of the phase from a strike-slip mechanism is much more complex then the nearly elliptical particle motion from the trust.

puting synthetic seismograms in a radially-symmetric structure and comparing them with our observations. Since all four events with a peculiar phase in the Love arrival window have near-nodal $R1$ phases, to verify our adapted version of PA5, we used two large events with source mechanism oriented to excite $R1$ of significant amplitude. Figure 7 illustrates good waveform fit for these two events in the Tonga region, one shallow (930516) and one deep (930416). Hypocentral parameters and mechanisms of these events are illustrated on Figure 3 and in Table 1.

Figure 8 compares synthetic seismograms of transverse and vertical components with data for the four events under investigation. While the overall match of major phases is quite good, some timing mismatches in the principal phases are obvious. They may reflect uncertainties in the location of these relatively small events. For three of the four events, the hypocentral depths were fixed to 15 km in the CMT computations. Discrepancies between the hypocentral locations published by the National Earthquake Information Center (NEIC) and CMT centroids suggest some uncertainty in locating these events. We found that for the thrust event 910108, using a depth value of 43 km (from the NEIC catalog) yielded a significantly better fit to the KIP record than the CMT depth of 15 km. Effects of lateral heterogeneity along the Tonga-Hawaii corridor may play a role as well.

Data from the strike-slip events, located ~200 km west of the thrust events, are fit better if the value of E is increased relative to that computed directly from the PA5 model. This change (from E=0.04, corresponding to S anisotropy of 4%, to E=0.06, corresponding to S wave anisotropy of 6%) yields a better fit to the time difference between the Raleigh and Love phase groups. Alternatively, a similar change in timing may be achieved by relocating both events farther away from the observation point.

Overall, synthetic seismograms computed in a radially symmetric structure represent major features of the observed wave field faithfully, including the shape and amplitude of the phase that precedes Rayleigh waves for both thrust events (910108 and 970330). Vertical synthetics for strike-slip events (910406 and 961116) conspicuously lack a body wave in the Love wave time window, leaving the observed phase unmodeled with a one-dimensional (1-D) structure. Recognizing that CMT source parameters are derived in least squares fit to data from a sparse global network of stations, we investigated the influence of possible errors in the centroid solution. Specifically, we computed synthetic seismograms for a variety of source mechanisms that deviated from the CMT solution by ±10° in strike, dip, and rake and by 10 and 25 km in source depth. We found that no combination of these perturbations to the source location and parameters would yield a synthetic seismogram with observed features.

To summarize, our computations in a 1-D velocity model show that in case of a shallow strike-slip source mechanism, the observed $P-SV$-polarized phase cannot be fully explained by the body waves of multiple S type. While these body waves probably are present in the seismogram at low amplitude, for strike-slip mechanisms their contribution to the vertical/radial motion in the Love time window is quite small.

5. Mode-Converted Surface Waves in a 2-D Structure

An alternative explanation for our observations would be a quasi-Love phase (qL) [*Yu and Park,* 1994; *Yu et al.* 1995; *Park and Yu,* 1993] that arises through mode conversion of the long-period Love wave at strong lateral

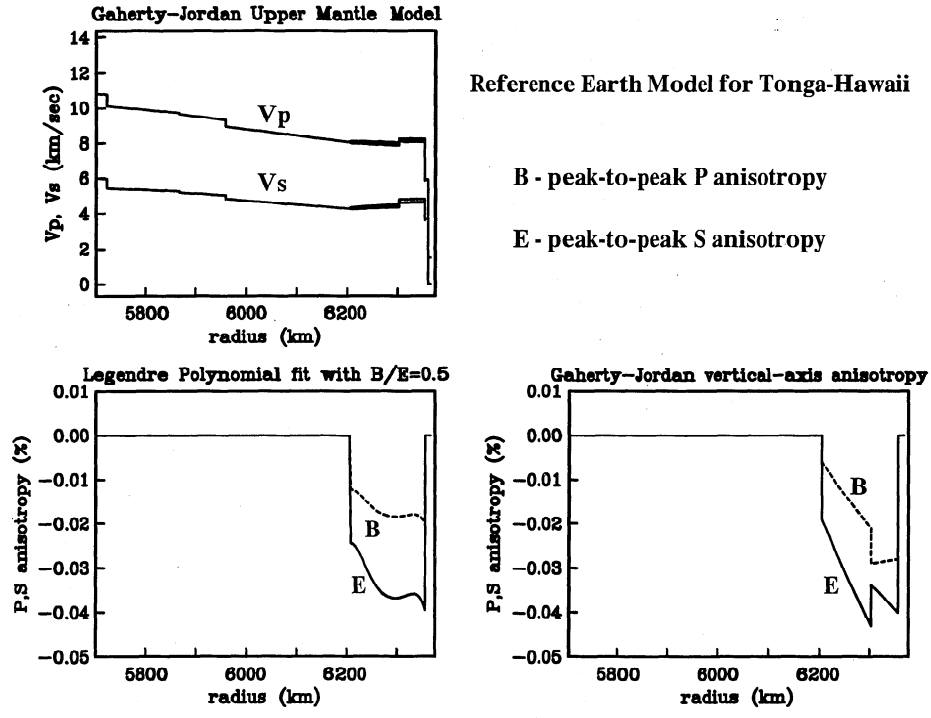

Figure 5. Vertical profiles of velocity and anisotropy in the model used for synthetic seismogram computation. Adapted from the PA5 model of *Gaherty et al.* [1996].

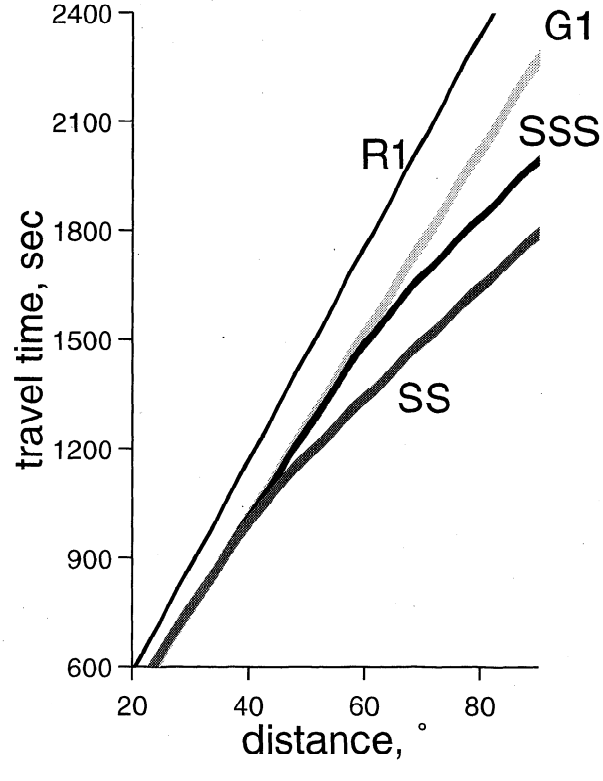

Figure 6. Travel time curves for surface and multiple body waves in IASPEI91 model.

gradients of upper mantle anisotropy. For upper mantle surface waves the effect of both isotropic lateral structure and surface topography on spheroidal-toroidal coupling appears to be weak. *Yu and Park* [1994] demonstrated the weak influence of sharp isotropic gradients in the upper mantle on qL waves. *Park and Yu* [1993] demonstrated the weak influence of surface topography for a model of the Kermadec arc/trench with 10 km of total relief. Although Hawaii swell topography is one-sided and somewhat broader, we expect the Kermadec computations to apply. The qL phases have been documented in the records of Hawaiian stations [*Desai et al.*, 1997; *Yu and Park*, 1994] at a wide range of back azimuth, suggesting an origin related to mantle flow local to the Hawaiian plume. Generated by Love-Rayleigh interaction, asymptotic coupling theory [*Park*, 1997] predicts that forward qL scattering along the great circle path is weak for lateral variations in either isotropic structure (parameters A and D in (1)) or in "radial anisotropy", i.e., media with a vertical axis of symmetry. Unlike the body wave discussed above, the qL phase does not arise from adjustments to radially symmetric structures but rather from lateral variations in "azimuthal anisotropy" along the propagation path.

For free oscillations ${}_nS_l$ (spheroidal/Rayleigh) and ${}_{n'}T_{l'}$ (toroidal/Love), the coupling interaction that leads to qL scattering is dominated by anisotropic structure

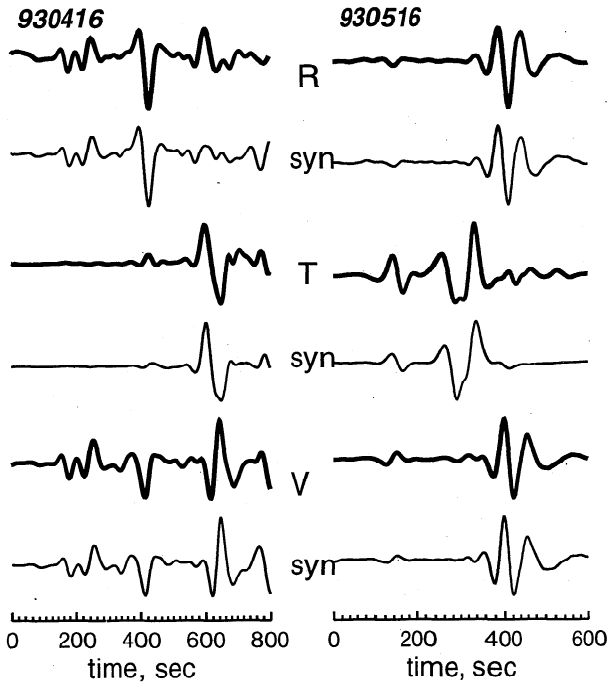

Figure 7. Waveform fit achieved in the adjusted PA5 model for two large earthquakes in the study area. Bold lines represent data; solid lines represent synthetics. Tracewise scaling is employed. Low-pass filter at 0.02 Hz is applied to all waveforms. This successful test of the model was performed to ascertain fair representation of SV-polarized phases.

with angular wavenumber $s = |l - l'|$ along the source-receiver great circle [*Park*, 1997]. For the fundamental dispersion branches ${}_0S_l$ and ${}_0T_{l'}$, the value of $|l - l'|$ varies from 1 at $f \approx 4$ mHz (250 s), to 21 at $f \approx 20$ mHz (50 s). Therefore long-period fundamental mode Love-to-Rayleigh forward scattering has the potential to resolve lateral variations in upper mantle anisotropy up to $s \approx 20$. This corresponds to 2000-km wavelength, or a 500-km-wide (i.e., a quarter of a cycle) gradient zone.

The largest Love/Rayleigh scattering arises from terms of the elastic tensor that are maximal for a horizontal symmetry axis $\hat{\mathbf{w}}$ oriented at $\xi = \pm 45^o$ azimuth to the source-receiver path or are maximal for an axis $\hat{\mathbf{w}}$ tilted between horizontal and vertical at $\xi = \pm 90^o$ azimuth to the path [*Park*, 1997]. Asymptotic theory predicts that the amplitude of an anisotropic gradient trades off with the azimuth angle ξ of $\hat{\mathbf{w}}$ for both groups of components within the elastic tensor. Specifically, for a given spatial wavenumber s, horizontal $\hat{\mathbf{w}}$, and compressional anisotropy parameter B the amplitude of a "quasi-Love" scattered wave scales with the product $B \sin 2\xi$. For a given scattered-wave amplitude, minimal anisotropy is required for $\xi = \pm 45°$. If $\xi = 15°$ or $\xi = 75°$, twice as much anisotropy is needed to cause the same cross-branch interaction. The path-integral asymptotics also predict that the coupling effects of shear and compressional anisotropies tend to cancel. Horizontal flow in olivine leads to a larger degree of anisotropy in P wave velocity relative to the S wave velocity regardless of the assumed mechanism of deformation [*Karato*, 1989]. Ophiolite samples measured by *Peselnick and Nicolas*, [1978] also yield higher anisotropy in P velocity. Several Earth models with radial anisotropy, such as PA5 and PREM, do not follow this observation, with S anisotropy parameterized as larger. Factors besides olivine alignment, such as fine layering in the upper mantle, could be the cause of this discrepancy. In our waveform tests we use radial anisotropy with S type dominant, i.e., that of PA5. We assume pure P-type azimuthal anisotropy as this leads to a minimal perturbation. The oceanic mantle, however, is likely to possess S anisotropy as well, so the true anisotropy is probably larger than our best fitting models.

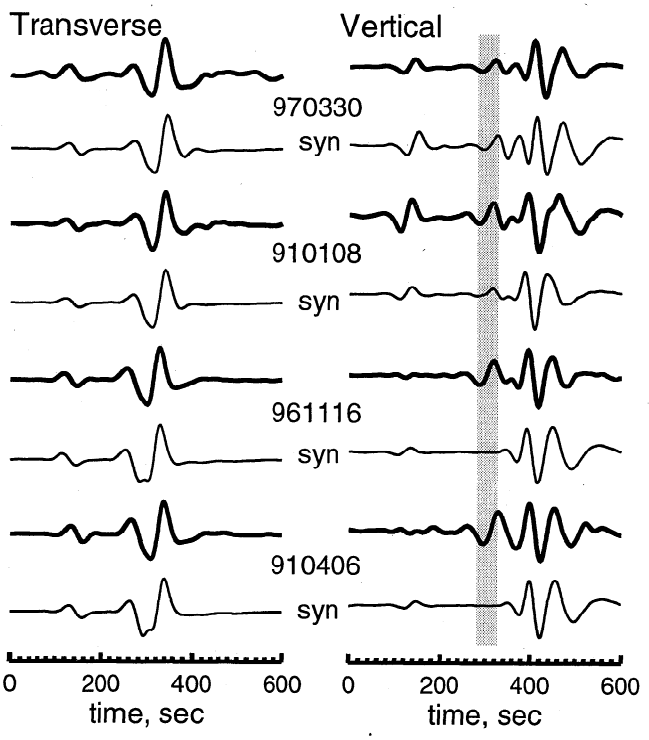

Figure 8. A comparison between data and synthetics in radially symmetric model PA5. Bold lines represent data; solid lines represent synthetics. Tracewise scaling is employed. Lowpass filter at 0.02 Hz is applied to all waveforms. The light grey vertical bar represents the time frame of SS phase arrival, widened at 40° due to a triplication in the travel time curve. Transverse component waveforms are matched for all four events, while vertical observations are reproduced for events with thrust mechanisms only (910106 and 970330). A conspicuous lack of energy prior to $R1$ on vertical components of events 940106 and 961116 suggest that in the case of a shallow strike-slip mechanism, the observed waveforms are mode-converted quasi-Love waves (qL), not body waves of the SS group.

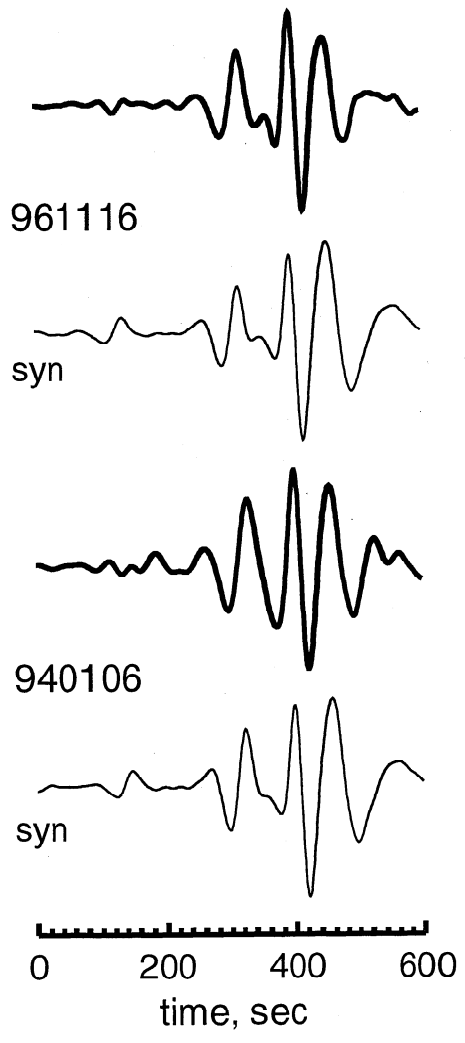

Figure 9. Vertical data traces (bold) compared with synthetic seismograms (solid) computed in the laterally inhomogeneous anisotropic velocity model schematically depicted in Figure 10. Tracewise scaling is employed. Low-pass filter at 0.02 Hz is applied to all waveforms.

Through trial-and-error forward modeling, we found that a phase similar to the observed ones arises for models that contain a step-like change in the orientation of anisotropy close to Hawaii. In the vertical components of data and synthetics for events 910406 and 961116 (Figure 9) the waveform ahead of the $R1$ phase is well matched in both cases. A discrepancy in the appearance of the 961116 and 910406 waveforms is not reproduced in the synthetics and thus is not simply a function of the event size (see Table 1) but likely arises from differences in the near-nodal $R1$ excitation.

The model yielding these synthetics is illustrated schematically in Figure 10. It is built by superimposing a laterally varying anisotropic structure onto the PA5 model adjusted as discussed above. Anisotropy in this additional structure is 6%, with a horizontal axis oriented at 45° to the propagation path. The timing of the phase is best matched if this additional anisotropy is present only within 3–5° from the station. Laterally varying anisotropy in a layer between 12 and 166 km (a depth range identical to the vertical axis anisotropy of the PA5 model) fits the observations.

The model presented is just one of the family of possible lateral anisotropic structures. Owing to the nature of mode interaction described above, certain anisotropic parameters exert competing influence on the resulting waveform, leading to trade-offs in modeling. Figure 11 documents the influence of some model parameters on synthetic seismograms. The location of the stepwise anisotropic gradient controls the timing of the resulting qL phase, as well as the shape of the waveform (Figure 11a). The timing of the observed qL phase, close on the heels of the Love arrival, argues for a sharp gradient near Hawaii, while its simple shape suggests that there are no sharp gradients elsewhere in the Tonga-Hawaii corridor. Anisotropy in P and S velocities have opposing effects, yielding waveforms of reversed polarity (Figure 11b). A combination of P and S anisotropy results in reduced amplitude of the qL phase. A symmetry axis at 45° to the path maximizes the qL waveform, with smaller and larger angles yielding progressively smaller qL phases (Figure 11c). Changing the axis-path angle from 45° to 15° or 75° rreduces the amplitude of a resulting qL phase by half. Additional complexity offered by an orthorhombic anisotropy model might enhance coupling effects [*Martin and Thomson,* 1997] and reduce the overall magnitude of velocity anisotropy required to fit the data. The amplitude of the qL phase is proportional to the thickness of the anisotropic layer (Figure

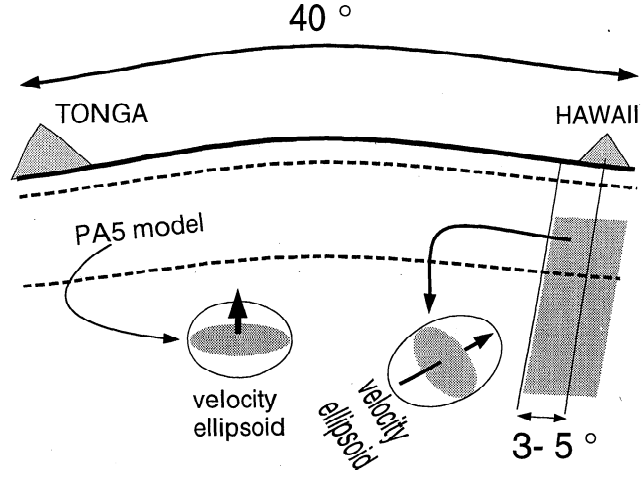

Figure 10. A schematic depiction of the velocity model sufficient to produce matching qL waveforms for our strike-slip events. The model is built as a perturbation to PA5 [*Gaherty et al.*, 1996]. In addition to the radial "slow" anisotropy of PA5, there is an area of azimuthal "fast" P only anisotropy of 6%, with horizontal symmetry axis oriented at 45° to the propagation path. The vertical boundary limiting an area of additional anisotropy is located 3-5° from the station. See text and Figure 11 for discussion of specific model parameters.

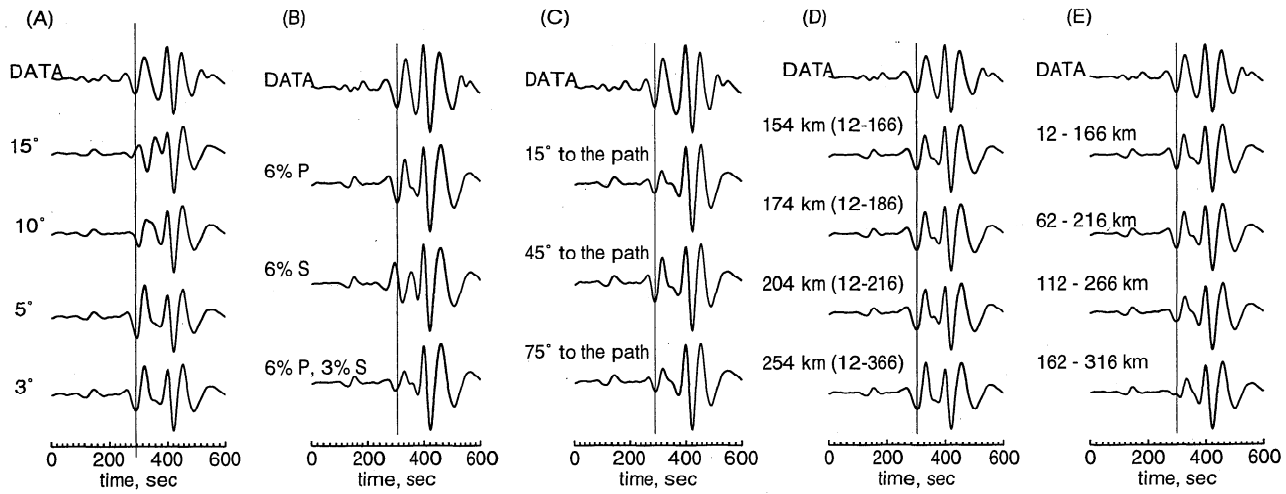

Figure 11. The sensitivity of qL to various model parameters. In each column the data trace (the vertical component of record 910406) is at the top, all other traces are synthetics. Low-pass filter at 0.02 Hz is applied to all waveforms. *(a)* Distance between the anisotropic gradient and the observation point (marked on synthetic traces) influences both the relative timing of the qL phase and its shape. If the gradient is farther than 15° from KIP, qL phase arrives late enough to blend with $R1$. (b) P and S anisotropy yield qL phases of opposite polarity. If both types of anisotropy are present in the model, and have identical "fast" polarity, the overall amplitude of the qL phase is smaller. (c) The angle between the path and the symmetry axis affects the amplitude of the resulting qL phase, with 45° yielding the largest effect. (d) The amplitude of the pulse scales with the thickness of the anisotropic layer. (e) The depth of the anisotropic layer influences the shape of the pulse.

11d). The depth of the layer affects both the amplitude and shape of the waveform (Figure 11e). This last comparison is most important, as it indicates that the layer with azimuthal anisotropy can be placed beneath the 11–68-km lithospheric lid of model PA5 with no changes in other parameters, but that deeper placement of this layer degrades the waveform fit significantly.

6. Discussion

For Tonga events of a thrust nature that occur at depths of 30-40 km the observed SV-polarized phase is well matched by a superposition of body phases (SS, $SnSn$). Tonga events of a strike-slip nature tend to be shallow (CMT depths of 15 km or less), and P-SV excitation is insufficient to generate body waves comparable in amplitude with observed signals. We are therefore led to conclude that for strike-slip events, Love-to-Raleigh scattering is the most likely cause of the observed waveform. This implies that the path from Tonga to Hawaii contains a significant gradient in the anisotropic properties of the mantle.

Locating this gradient in close proximity to Hawaii would preserve agreement with previous studies of the anisotropic structure in this region of the Pacific. The study of the Tonga-Hawaii corridor by *Gaherty et al.* [1996] modeled P-SV and SH dispersion discrepancies with radial anisotropy, leading to model PA5. In the region nearby, *Su and Park* [1994] identified horizontal axis S wave anisotropy that imposes 1.8 s of splitting onto $P-S$ converted phases, with fast axis perpendicular to the Tonga-Hawaii corridor. *Gaherty et al.*, [1996] note that this orientation of azimuthal anisotropy would leave SH and SV particle motion unmixed and could be used as an alternative to the radial anisotropy of PA5. Long-period Love and Rayleigh motions do not couple strongly either for a vertical axis of symmetry or for a fast axis oriented perpendicular to Tonga-Hawaii path. This again suggests that any Love-Rayleigh scattering observed at Hawaii should be related to azimuthal anisotropy gradients local to Hawaii. Our laterally varying model contains no azimuthal anisotropy along most of the Tonga-Hawaii corridor. If azimuthal, rather than radial, anisotropy is assumed to be the cause of the observations modeled by *Gaherty et al.* [1996], a sharp gradient in azimuthal anisotropy close to Hawaii would still be required to fit the qL phases we have identified.

The model we propose places a change from the radial anisotropy to a combination of radial and azimuthal anisotropy at a distance of 330-550 km from Hawaii. This distance is consistent with the timing of the qL phase relative to Love. The lack of complexity in the qL phase argues against the existence of multiple scattering points along the Tonga-Hawaii corridor. We note, however, that scattered waves generated close to the source, perhaps associated with mantle flow proximal to the Tonga slab edge, would be difficult to distinguish visually from the near-nodal Rayleigh wave. It is natural to associate this change with the influence of the hot spot-related flow pattern in the upper mantle. In the model

suggested by *Ribe and Christensen* [1994], the hotspot-induced disruption of the ambient mantle flow follows a "stagnation streamline" that bounds the the Hawaiian swell. Since their theoretical model predicts a somewhat wider topographic disturbance than is observed, we identify the orientation of the stagnation streamline with the 5100 m isobath on Figure 1, approximately where our modeling indicates a strong lateral gradient in anisotropic properties. Since this isobath intersects the Tonga-KIP path at roughly $\xi = 75°$, an exact alignment of the anisotropy axis with the flow line seems plausible only if we allow for a large (10%) amount of anisotropy and/or for a horizontally anisotropic layer that is 200-300 km thick.

An interpretation purely in terms of hot spot mantle flow becomes less tenable if we accept the simplest model obtained from our waveform synthetics, namely, uniform azimuthal anisotropy between 12 and 166 km depth in model PA5. This depth range includes both the upper asthenosphere and the lithospheric lid. Anisotropy in the lithospheric lid is not likely to be induced directly by the upwelling hot spot flow, as 3-D thermomechanical modeling of plume-lithosphere interaction by *Ribe and Christensen* [1994] indicates that lithospheric "erosion" is minimal. Alternatively, the ascent of basaltic melts through porous peridotite could leave an anisotropic imprint on nominally undeformed oceanic lithosphere. Numerous studies of ophiolites have reported "residual dunite" bodies on length scales of 1 cm to 100 m, thought to represent conduits for upward flow of basaltic melt [*Nicolas*, 1989]. These tabular olivine-rich conduits are thought to develop because basaltic melts interact with the porous wall rock to induce orthopyroxene melting and olivine crystallization, if the melt is close to the peridotite solidus [*Kelemen*, 1990]. Field evidence suggests strong olivine crystal alignment in residual dunites is common, due primarily to recrystallization in the presence of upward magma flow [*Kelemen and Dick*, 1995]. Though not specifically required by our data analysis (Figure 11), residual-dunite recrystallization may influence anisotropy in the lid here and near other sites of marine volcanism.

It should be noted that a simple plume flow pattern, like that envisioned by *Ribe and Christensen* [1994], may not necessarily apply. Strong qL converted phases arrive at KIP from the direction subparallel to the Hawaiian-Emperor chain [*Desai et al.*, 1997], suggesting significant anisotropic gradients where the symmetry of a simple plume model would predict little or no Love-Rayleigh coupling. A 2-D tomographic image of the Tonga-Hawaiian path based on shear wave data prompted *Katzman et al.* [1998] to dispense with the plume idea altogether in favor of a more extensive upper mantle flow pattern, with velocity variations induced by partial melting. Other plume-flow models are possible, however. To explain volcanic seamounts in en echelon segments along the Hawaii-Emperor hot spot track, as well as geochemical differences among Hawaiian volcanos, *Ihinger* [1995] argued for intermittent plumelets drifting in an ambient upper mantle return flow, oblique to the nominal hotspot track. Flow in the sublithospheric mantle in Ihinger's kinematic model is oriented 50° south of east with respect to the Hawaii hot spot, roughly 30° clockwise of the strike defined by the Hawaiian island/seamounts chain. This orientation is more conducive to Love-Rayleigh scattering on the Tonga-Hawaii corridor than the standard hot spot model, that is, it would require a smaller jump in anisotropic properties to model the qL observations.

Numerous trade-offs among parameters of our model require final interpretation on the basis of "external" data. For example, anisotropy in either P wave velocity or S wave velocity results in qL phase development, but of opposite polarities. Clearly, one type of anisotropy must dominate to produce the observed effect. P velocity anisotropy is believed to be more pronounced in deformed peridotites [*Karato*, 1989; *Anderson*, 1989], and thus our choice of the NW-SE alignment of the anisotropic symmetry axis is controlled by the effect of P anisotropy. The upper and lower depth bounds of the proposed horizontal anisotropy layer have considerable uncertainty (see Figures 11d and 11e). Nevertheless, a need for such anisotropy in the upper 200 km of the mantle is quite well established. Placing the upper bound of the layer below 150 km leads to a considerable mismatch of synthetics and data. As the thickness of the layer is in direct trade-off with the amount of anisotropy, an independent constraint on the amount of anisotropy (e.g., from a refraction experiment like the Ngendie by *Shearer and Orcutt* [1986]) would greatly reduce the range of possible models.

Acknowledgments.
We used **GMT** software [*Wessel and Smith*, 1991] to prepare figures. Detailed description of the PA5 model was obtained from the website maintained by J. Gaherty. J. Gaherty, G. Laske, and M. Kendall provided valuable comments in review. Supported by NSF grant EAR-9507990.

References

Anderson, D. L., *A Theory of the Earth*, Blackwell Sci., Malden, Mass.,1989.

Backus, G. E., Possible forms of seismic anisotropy of the uppermost mantle under oceans, *J. Geophys. Res., 70*, 3429–3439, 1965.

Desai, B., J. Park and V. Levin, Seismic anisotropy and mantle flow near the Hawaii hot spot (abstract), *Eos Trans. AGU, 78 (46), Fall Meet. Suppl.*, F500–F501, 1997.

Dziewonski, A. M., and Anderson, D., Preliminary reference Earth model, *Phys. Earth Planet. Inter.*, , *25*, 297–356, 1981.

Gaherty, J. B., T. Jordan, and L. S. Gee, Seismic structure of the upper mantle in a central Pacific corridor, *J. Geophys. Res., 101*, 22291–22309, 1996.

Helsley, C. E., and M. B. Steiner, Evidence for long intervals of normal polarity during Cretaceous period, *Earth Planet. Sci. Lett.*, , *5*, 325-332, 1969.

Ihinger, P. D., Mantle flow beneath the Pacific Plate: evi-

dence from seamount segments in the Hawaiian-Emperor chain, *Am. J. Sci., 295*, 1035–1057, 1995.

Jordan, T. J., A procedure for estimating lateral variations from low-frequency eigenspectral data, *Geophys. J. R. Astron. Soc., 51*, 441–455, 1978.

Jordan, T. J., and S. A. Sipkin, Estimation of the attenuation operator for multiple ScS waves, *Geophys. Res. Lett., 4*, 167–170, 1977.

Karato, S., Seismic anisotropy; mechanisms and tectonic implications, in *Rheology of solids and of the Earth*, pp 393-422. Oxford Univ. Press, New York, 1989.

Katzman, R., L. Zhao, and T. H. Jordan, High-resolution, two-dimensional vertical tomography of the central Pacific mantle using *ScS* reverberations and frequency-dependent travel times, *J. Geophys. Res., 103*, 17933–17971, 1998.

Kelemen, P. B., Reaction between ultramafic rock and fractionating basaltic magma, I, Phase relations, the origin of calc-alkaline magma series, and the formation of discordant dunite, *J. Petrol., 31*, 51–98, 1990.

Kelemen, P. B., and H. J. B. Dick, Focused melt flow and localized deformation in the upper mantle: Juxtaposition of replacinve dunite and ductile shear zones in the Josephine peridotite, SW Oregon, *J. Geophys. Res., 100*, 423–438, 1995.

Martin, B. E., and C. J. Thomson, Modeling surface waves in anisotropic structures; II Examples. *Phys. Earth Planet. Inter.*, , 103, 253–279, 1997.

McNutt, M. and K. Fischer, The South Pacific Superswell, in *Seamounts, Islands and Atolls, Geophys. Monogr. Ser.* vol. 43, edited by B. Keating et al., pp 25–34, AGU, Washington, D.C., 1987.

Menard, H. W., 1984. Darwin reprise, *J. Geophys. Res., 89*, 9960–9968.

Nicolas, A., *Structures of Ophiolites and Dynamics of Oceanic Lithosphere*, Kluwer Acad., Norwell, Mass., 1989.

Park, J., Asymptotic coupled-mode expressions for multiplet amplitude anomalies and frequency shifts on an aspherical Earth, *Geophys. J. R. Astron. Soc., 90*, 129–169, 1987.

Park, J., The sensitivity of seismic free oscillations to upper mantle anisotropy, I, Zonal structure, *J. Geophys. Res., 98*, 19933–19949, 1993.

Park, J., Free oscillations in an anisotropic earth: Path-integral asymptotics, *Geophys. J. Int., 129*, 399–411, 1997.

Park, J., Path-integral synthetic seismograms for an anisotropic upper mantle, *Geophys. J. Int.*, in press, 1998.

Park, J., and Y. Yu, Anisotropy and coupled free oscillations: Simplified models and surface wave observations, *Geophys. J. Int., 110*, 401–420, 1992.

Park, J., and Y. Yu, Seismic determination of elastic anisotropy and mantle flow, *Science, 261*, 1159–1162, 1993.

Peselnick, L., and A. Nicolas, Seismic anisotropy in an ophiolite peridotite: application to oceanic upper mantle, *J. Geophys. Res., 83*, 1227–1235, 1978.

Renkin, M. L., and J. G. Sclater, Depth and age in the North Pacific, *J. Geophys. Res., 93*, 2919–2935, 1988.

Revenaugh, J., and T. H. Jordan, Observations of first-order mantle reverberations, *Bull. Seismol. Soc. Am., 77*, 1704–1717, 1987.

Ribe, N. M., and U. R. Christensen, Three-dimensional modeling of plume-lithosphere interaction, *J. Geophys. Res., 99*, 669–682, 1994.

Shearer, P. M., and J. A. Orcutt, Compressional and shear wave anisotropy in the oceanic lithosphere, The Ngendie seismic refraction experiment, *Geophys. J. Int., 87*, 967–1003, 1986.

Smith, M. F., and F. A. Dahlen, The azimuthal dependence of Love and Rayleigh wave propagation in a slightly anisotropic medium, *J. Geophys. Res., 78*, 3321–3333, 1973.

Stein, C., and S. Stein, Constraints on Pacific midplate swells from global depth-age and heat-flow age models, in *The Mesozoic Pacific; geology, tectonics, and volcanism, Geophys. Monogr. Ser.* vol. 77, edited by M. Pringle, pp 53–76, AGU Washington, D.C., 1993.

Su, L., and J. Park, Anisotropy and the splitting of PS waves, *Phys. Earth Planet. Inter., 86*, 263–276, 1994.

Su, L., J. Park, and Y. Yu, Born seismograms using coupled free oscillations: The effects of strong coupling and anisotropy, *Geophys. J. Int., 115*, 849–862, 1993.

Wessel, P., and W. H. F. Smith, Free software helps map and display data, *Eos Trans. AGU, 72*, 441, 445-446, 1991.

Yu, Y., and J. Park, Hunting for azimuthal anisotropy beneath the Pacific Ocean region, *J. Geophys. Res., 99*, 15399–15421, 1994.

Yu, Y., J. Park, and Wu, F., Mantle anisotropy beneath the Tibetan Plateau: evidence from long-period surface waves, *Phys. Earth Planet. Inter., 87*, 231–246, 1995.

V. Levin and J. Park, Department of Geology and Geophysics, Box 208109, Yale University, New Haven CT 06520. (e-mail: vadim@hess.geology.yale.edu; park@hess.geology.yale.edu)

(Received December 30, 1997; revised May 14, 1998; accepted July 6, 1998.)